

# On the Thermodynamic Stability of Confined Thin Films Under Shear

Dennis J. Diestler, Martin Schoen, John H. Cushman

Thin films of monatomic fluid constrained between two plane-parallel structured solid walls have been modeled by Monte Carlo simulation under conditions (fixed temperature, chemical potential, and normal stress or load) prevailing in high-precision measurements of surface forces. Several states of the film, corresponding to different numbers of layers of fluid parallel with the walls, are generally consistent with these conditions, but only one is thermodynamically stable; the others are metastable. When the walls are properly aligned, epitaxial solid phases are stable. These melt under shear, eventually becoming metastable, whereupon a drainage (or imbibition) transition occurs, leading to a stable phase with fewer (or more) layers.

The behavior of confined fluids, which figures prominently in such disparate phenomena as the swelling of clay soils (1), transport in biological membranes (2), and lubrication (3), can be studied directly on a molecular scale under precisely controlled conditions in the surface forces apparatus (SFA) (4–6). The heart of the SFA is a slit pore consisting of two plane-parallel solid surfaces or walls (normally atomically smooth mica sheets) separated by a film of the fluid of interest. One wall is fixed and the other is attached to a movable stage, which allows the relative position and alignment of the walls to be manipulated and measured with molecular precision. The slit pore is immersed in the bulk fluid, which is maintained at fixed temperature ( $T$ ) and pressure ( $p$ ), so that the chemical potential ( $\mu$ ) of the bulk fluid is also fixed. The film and bulk phases are taken to be in thermodynamic equilibrium; the temperature and chemical potential of the film are therefore also fixed at the bulk values. We present the results of Monte Carlo simulations of the SFA.

If a molecularly thin film is subjected to a shear strain under fixed normal stress or load  $\tau_3$  (say, by moving one wall laterally relative to the other), then the shear stress rises nearly linearly until a critical strain is reached; it then falls precipitously as the critical point is exceeded. As shearing continues, this “stick-slip” cycle recurs, giving rise to a saw-tooth-shaped plot of shear stress versus strain (6). This static stick-slip phenomenon has also been observed in previous Monte Carlo (7) and molecular dynamics (8, 9) simulations of a prototypical model of the slit pore described below. These computations show directly that a

monatomic fluid piles up in layers parallel with the walls. Moreover, if the walls are aligned properly, they can induce the formation of an epitaxial solid, which resists shearing (walls stick) until a critical shear strain is exceeded (that is, until the walls are moved sufficiently out of alignment), whereupon the solid melts (walls slip). When the walls again come into proper alignment, the cycle repeats itself. This sort of stick-slip behavior is characteristic of molecularly thin films of relatively simple materials (small organic molecules) constrained between atomically smooth mica walls that are subjected to small shear-strain rates.

We use a simple prototypical model of the slit pore: a monatomic fluid constrained between walls composed of like atoms fixed rigidly in the configuration of the (100) plane of the face-centered-cubic (fcc) lattice. We take the potential energy of the system to be a pairwise sum of Lennard-Jones (6, 12) intermolecular potentials  $u(r) = 4\epsilon[(\sigma/r)^{12} - (\sigma/r)^6]$ , where  $r$  is the distance between atoms of a given pair. Reduced dimensionless variables (denoted by an asterisk) are defined in terms of the well depth  $\epsilon$  and the molecular “diameter”  $\sigma$ ; distance is given in units of  $\sigma$ , energy in units of  $\epsilon$ , temperature in units of  $\epsilon/k_B$ , where  $k_B$  is Boltzmann’s constant, and stress (pressure) is given in units of  $\epsilon/\sigma^3$ . We take the walls to be parallel to the  $xy$  plane and to be a distance  $h$  apart. To minimize edge effects, we impose periodic boundary conditions in the  $x$  and  $y$  directions on a rectangular prism (lamella) of fluid having lateral dimensions  $s_x = s_y = s$ , where  $s$  is taken to be sufficiently large ( $s^* = 7.9925$ ) that intensive properties of the system do not depend on  $s$ . The alignment of the walls in the  $x$  direction is specified by the registry  $\alpha$ , which relates the  $x$  coordinates of corresponding wall atoms by  $x_2 = x_1 + \alpha\ell$ , where  $0 \leq \alpha \leq 0.5$  and  $\ell$  is the lattice constant of the two-dimensional unit cell

of the fcc (100) plane. For simplicity, the alignment in the  $y$  direction is kept fixed.

The shear-strain rate used in the actual SFA is exceedingly low on a molecular scale ( $\sim 10^{-8}$  Å/ps). We therefore assume that the process is reversible and apply the Monte Carlo method in a statistical ensemble to which we shall refer as the grand-isostress (GI) ensemble or  $(\mu, T, \text{ and } \tau_3)$  ensemble, the latter designation indicating the experimentally controlled thermodynamic variables that are the parameters of the ensemble. Previous simulations (7–10) have not taken proper account of the drainage (or imbibition) of fluid that can occur under shearing at constant  $\mu, T, \text{ and } \tau_3$ . The details of the GI Monte Carlo method are given elsewhere (11). Here, we merely describe the implementation.

The oscillations in  $\tau_3^*$  (Fig. 1) reflect the addition (imbibition) or removal (drainage) of whole layers of fluid as  $h^*$  varies. That the isobars  $\tau_3^* = \text{constant}$  intersect the  $\tau_3^*$  versus  $h^*$  curve at several distinct values of  $h^*$  suggests that a number of different thermodynamic states (corresponding to different numbers of layers) are possible for given conditions of fixed  $\mu^*, T^*, \text{ and } \tau_3^*$ . However, only one of these states is thermodynamically stable; the others are metastable. The stable state is the one for which the GI potential

$$\begin{aligned} \phi &= U - TS - \mu N - \tau_3 A h \\ &= \Omega - \tau_3 A h \end{aligned} \quad (1)$$

that is appropriate to the constraints of fixed  $T, \mu, \text{ and } \tau_3$  is at a minimum (11). In Eq. 1,  $U$  is the internal energy,  $S$  is the entropy, and  $N$  is the amount (number of molecules) of the pore fluid;  $A = s^2$  is the area of the wall.

From the first and second laws of thermodynamics and the definitions of  $\phi$  and the grand potential  $\Omega$  given in Eq. 1, we deduce expressions that govern infinitesimal, reversible transformations

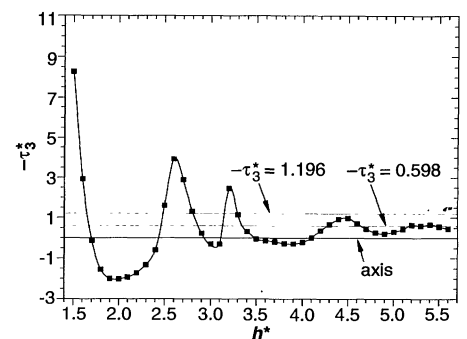


Fig. 1. Negative of applied normal stress ( $-\tau_3^*$ ) as a function of separation  $h^*$  between the walls of the fcc prototype at  $T^* = 1.00, \mu^* = -11.0$ , and  $\alpha = 0.0$ . The horizontal lines are isobars at  $\tau_3^* = -0.598$  and  $-1.196$ .

D. J. Diestler, Department of Agronomy, University of Nebraska, Lincoln, NE 68583.

M. Schoen, Institut für Theoretische Physik, Technische Universität Berlin, Hardenbergstr. 36, 10623 Berlin, Germany.

J. H. Cushman, Purdue University, West Lafayette, IN 47907.

$$d\Omega = -SdT - Nd\mu + (\tau_1 + \tau_2)(h/2) dA + \tau_3 Adh + \tau_4 Ad(\alpha\ell) \quad (2a)$$

$$d\phi = d\Omega - d(\tau_3 Ah) = -SdT - Nd\mu + \gamma dA - Ah d\tau_3 + \tau_4 Ad(\alpha\ell) \quad (2b)$$

Here  $\tau_1$  and  $\tau_2$  are the components of stress in the  $x$  and  $y$  directions applied to surfaces of the lamella that point in these directions,  $\tau_4$  is the shear stress applied to the walls in the  $x$  direction, and

$$\gamma = (\partial\phi/\partial A)_{T,\mu,\tau_3,\alpha} = h(\tau_1 + \tau_2 - 2\tau_3)/2 \quad (3)$$

is an interfacial tension analogous to ordinary surface tension.

Because the local density depends only slightly on  $x$  and  $y$ , it is tempting to treat the confined phase as if it were homogeneous in transverse dimensions. Were this so,  $\tau_1$  and  $\tau_2$  would be independent of  $A$  for given fixed  $T$ ,  $\mu$ ,  $\tau_3$ , and  $\alpha$ , and we could therefore integrate Eq. 2b to obtain

$$\phi = \gamma A \quad (4a)$$

or from Eqs. 1 and 3

$$\Omega = (\tau_1 + \tau_2)hA/2 \quad (4b)$$

Equation 4b is the analog of the bulk-phase relation  $\Omega = -pV$  ( $\tau_1 = \tau_2 = -p$ ) ( $V$  is volume). Although Eqs. 4a and 4b, are rigorously true for smooth-wall slit pores (12), their application to the structured-wall prototype can lead to qualitatively incorrect conclusions. The formation of epitaxial solid phases gives rise to a dependence of  $\tau_i$  on  $A$  sufficiently strong to preclude the proposed integration.

Fortunately, we require only relative values of  $\phi$  for our present purpose; we can obtain these by numerical integration of Eq. 2 at constant  $A$ . Thus, from the intersections of a given isobar  $\tau_3 = \text{constant}$  with the plot of  $\tau_3$  versus  $h$  (Fig. 1), we determine the values of  $h$  consistent with the given values of  $T$ ,  $\mu$ ,  $\tau_3$ , and  $\alpha$ . Choosing as a reference state the one-layer phase at  $\alpha = 0.0$ , we have for the potential of the  $i$ -layer phase

$$\Delta\phi_i = \Delta\phi_i^{(1)} + \Delta\phi_i^{(2)} \quad (5)$$

where

$$\Delta\phi_i^{(1)} = A \int_{h_1}^{h_i} \tau_3(h') dh' - A\tau_3(h_i - h_1) \quad (6a)$$

is the contribution accruing as the walls are moved reversibly from  $h_1$  to  $h_i$  at constant  $T$ ,  $\mu$ ,  $A$ , and  $\alpha = 0.0$ . The second term in Eq. 5, given by

$$\Delta\phi_i^{(2)} = A\ell \int_0^\alpha \tau_4(\alpha') d\alpha' \quad (6b)$$

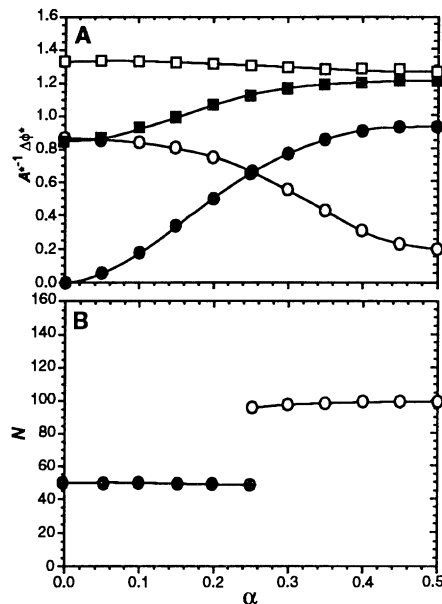


**Fig. 2.** (A) Relative GI potential per unit area ( $A^{-1}\Delta\phi$ ) as a function of registry  $\alpha$  for metastable phases of the prototype at  $T^* = 1.00$ ,  $\mu^* = -11.0$ , and  $\tau_3^* = -0.598$ : one-layer phase (●); two-layer phase (○); three-layer phase (■); and four-layer phase (□). (B) Number of molecules as a function of registry for the stable phase under the same conditions.

is the change in  $\phi$  accompanying the reversible change in registry at constant  $T$ ,  $\mu$ ,  $\tau_3$ , and  $A$ .

Using Eqs. 5 and 6, we construct plots of relative GI potential as a function of registry (Figs. 2A and 3A). The various curves refer to films comprising different numbers of layers, which vary between one and four under the assumed conditions. In all cases,  $T^* = 1.00$  and  $\mu^* = -11.0$ , which correspond to a bulk fluid state having density  $\rho^* = 0.7953$  and pressure  $p^* = 0.483$ . Two competing effects account for the order of stability of the confined phases as a function of normal stress and registry. First, increasing  $-\tau_3$  tends to squeeze fluid out of the pore, producing thinner films that are more stable. Second, when the walls are in registry ( $\alpha = 0.0$ ), phases with odd numbers of layers are generally more stable than those with even numbers of layers. The in-plane pair correlation function  $g^{(2)}$  (13) indicates that at  $\alpha = 0.0$ , the "odd-layer" phases are solid, whereas the "even-layer" ones are fluid. When the walls are out of registry, on the other hand, the even-layer phases (now solid) are more stable than the odd-layer ones (fluid). Thus, at the extremes of registry, the stable phases are odd- or even-layer solids. However, if  $-\tau_3$  is sufficiently large, the one-layer phase is stable at all registries.

Consider the stable one-layer phase at the lower normal stress (Fig. 2). To force the walls out of registry (that is, to in-

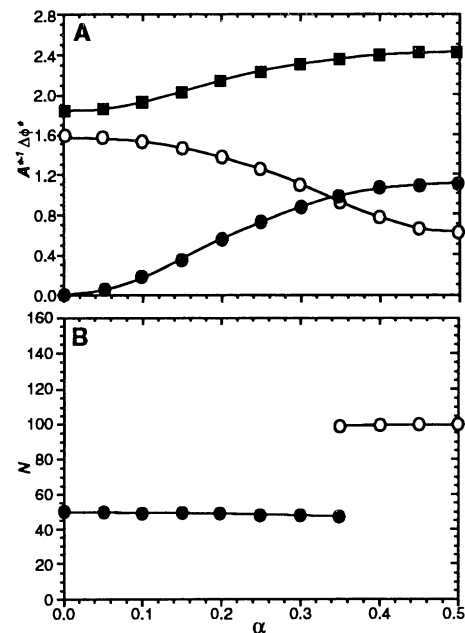


**Fig. 3.** (A) Relative GI potential per unit area and (B) number of molecules as Fig. 2, except  $\tau_3^* = -1.196$ .

crease  $\alpha$  from zero), one must do mechanical work on the confined solid by shearing it. As a result, the GI potential rises; the potential of the metastable two-layer phase simultaneously drops. In the vicinity of  $\alpha \sim 0.25$ , the potential curves cross, indicating that the two phases become equally stable. Just beyond  $\alpha \sim 0.25$ , the two-layer phase becomes the stable one. There is a sharp increase in the number of confined molecules (Fig. 2B) as the film goes through the imbibition transition around  $\alpha \approx 0.25$  to take on a second layer. The values of  $g^{(2)}$  for both phases are indicative of strained solids.

At the higher applied normal stress (Fig. 3), the picture is qualitatively similar. However, the three- and two-layer phases are now less stable relative to the one-layer phase than they are at the lower  $-\tau_3$  (Fig. 2). The four-layer phase has become unstable. A consequence of the decreased stability of the two-layer phase is a shift of the imbibition transition to higher registry ( $\alpha = 0.35$ ). Moreover, the one-layer phase becomes fluid before the transition ( $\alpha < 0.35$ ), according to  $g^{(2)}$ , whereas the two-layer phase is solid. Thus, from the opposite perspective, as  $\alpha$  decreases from 0.50, the two-layer solid film undergoes a shear melting transition (drainage) to produce a one-layer liquid film.

It is interesting that at zero normal stress, the three-layer solid is stable at  $\alpha = 0.0$  and undergoes a drainage transition to a two-layer phase in the range  $0.25 < \alpha < 0.30$ . The two-layer phase becomes solid at  $\alpha = 0.5$  (11).

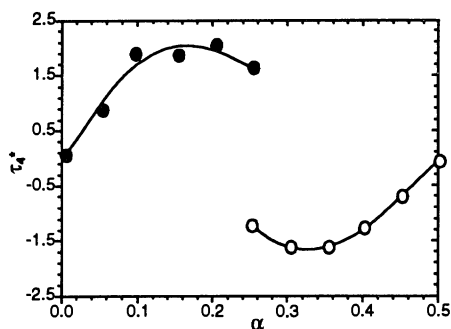


Fig. 4. Shear stress ( $\tau_4^*$ ) as a function of registry for stable phases under the conditions given in Fig. 2.

If the upper wall were permitted to float (under zero applied shear stress,  $\tau_4 = 0$ ) on the film, it would come to rest with a registry corresponding to the minimum of  $\phi$ . Under the conditions of our simulations,  $\phi$  is minimum at either  $\alpha = 0.0$  or  $0.5$ , where, respectively, odd- and even-layer solid films exist. For instance, at  $\tau_3^* = -0.598$  and  $-1.196$ , the one-layer solid at  $\alpha = 0.0$  is stable; at  $\tau_3^* = 0.0$ , the walls adjust so that  $\alpha = 0.5$  and the two-layer phase forms.

The shear stress  $\tau_4^*$  oscillates between positive and negative values as the film is sheared ( $\alpha$  increases) (Fig. 4). When the walls are in registry ( $\alpha = 0.0$ ), the stable phase is a one-layer phase, which resists shearing by exerting a force on the walls opposing the (positive) applied shear stress, that is, in the direction of decreasing  $\alpha$ . However, when  $\alpha$  exceeds a critical value, the imbibition transition yields the more stable two-layer phase. As  $\alpha$  increases beyond the critical value, the GI potential of the two-layer phase decreases. The strained phase now exerts a force on the walls in the direction of increasing  $\alpha$ , which gives rise to a negative applied shear stress. The periodic sharp drops in frictional force below the baseline observed in the "super-kinetic" sliding state of the SFA (14) may reflect alternating imbibition and drainage transitions analogous to the ones described here.

## REFERENCES AND NOTES

1. P. F. Low, *Langmuir* **3**, 181 (1987).
2. F. M. Etzler and W. Drost-Hansen, in no. 188 of the *Advances in Chemistry Series*, M. Blank, Ed. (American Chemical Society, Washington, DC, 1980), p. 486.
3. S. Granick, *Science* **253**, 1374 (1991).
4. J. N. Israelachvili, P. M. McGuiggan, A. M. Homola, *ibid.* **240**, 189 (1988).
5. J. van Alsten and S. Granick, *Phys. Rev. Lett.* **61**, 2570 (1988).
6. M. L. Gee, P. M. McGuiggan, J. N. Israelachvili, *J. Chem. Phys.* **93**, 1895 (1990).
7. M. Schoen, C. L. Rhykerd Jr., D. J. Diestler, J. H. Cushman, *Science* **245**, 1223 (1989).
8. P. A. Thompson and M. O. Robbins, *ibid.* **250**, 792 (1990); M. O. Robbins and P. A. Thomp-

9. M. Lupkowski and F. van Swol, *J. Chem. Phys.* **95**, 1995 (1991).
10. M. Schoen, D. J. Diestler, J. H. Cushman, *Phys. Rev. B* **47**, 5603 (1993).
11. D. J. Diestler, M. Schoen, J. H. Cushman, in preparation.
12. S. G. Ash, D. H. Everett, C. Radke, *Faraday Trans.* **2** **69**, 1256 (1973).
13. M. Schoen, D. J. Diestler, J. H. Cushman, *J. Chem. Phys.* **87**, 5464 (1987).

14. H. Yoshizawa, P. McGuiggan, J. Israelachvili, *Science* **259**, 1305 (1993).
15. This work was supported by the U.S. Department of Energy, Office of Health and Environmental Research (DE-FG02-86ER-60310), and the U.S. Army Research Office (DAAL03-90-G-0074). The authors are grateful for time on the CRAY Y-MP/832 of the Höchstleistungsrechenzentrum at the Forschungszentrum Jülich.

18 May 1993; accepted 8 September 1993

## Long-Range Attractive Force Between Hydrophobic Surfaces Observed by Atomic Force Microscopy

Yi-Hua Tsao, D. Fennell Evans, H. Wennerström

There is evidence from atomic force microscopy for a long-range attractive force between hydrophobic surfaces that is virtually identical to that observed with the surface forces apparatus. This force is present in the nonaqueous solvent ethylene glycol. A possible molecular mechanism involves in-plane polarized domains of solid-like monolayers adsorbed on mica, and a theoretical model has been developed that accounts for many of the observations.

Hydrophobic interactions guide molecular self-assembly processes in biology and in many technological processes. It is known that hydrophobic interactions are proportional to the contact area both on the molecular and the colloidal (macroscopic) scale. However, little is known about the range of the hydrophobic forces, which is an important point in understanding the dynamics of self-organizing processes such as protein folding, ligand binding to hydrophobic receptor sites, and the transformation of membrane structures.

Reports published over the past decade (1–5) document the existence of long-range, strongly attractive forces between macroscopic hydrophobic surfaces immersed in water. These forces are orders of magnitude larger than that expected from van der Waals interactions and exhibit decay lengths of up to 25 nm. The molecular origin of these unusual forces is not well understood. None of the proposed mechanisms—which include water structural effects (2), Debye screened ion-ion or dipole-dipole correlations (6, 7), or vapor cavitation (3)—account for the experimental observations. At issue is the question of whether these long-range attractive forces arise from hydrophobic interactions and whether they provide an additional attractive force that promotes biomolecular processes.

To date, all accurate measurements of this force have been made with the surface forces apparatus (SFA), for which hydrophobic sur-

faces are prepared by the deposition of a monolayer of a double-chained cationic surfactant onto a negatively charged mica surface. Here, we (i) give a brief review of previous SFA measurements; (ii) present results of atomic force microscopy (AFM) showing the existence of the long-range force for equivalent systems; (iii) establish the existence of a long-range attractive force in a nonaqueous solvent, ethylene glycol; (iv) investigate other hydrophobic surfaces, such as Teflon and polyethylene; and (v) propose a model that explains the molecular origin of the long-range attractive force.

Both the magnitude and the range of the long-range attractive force between two hydrophobic surfaces in water depend on the temperature and length of the surfactant's hydrocarbon chain. The SFA results (5) at 25°C (Fig. 1A) show that dioctadecyldimethylammonium (DODA), dieicosyldimethylammonium (DEDA), and didoeicosyldimethylammonium (DDDA) monolayers gave identical results, whereas the dihexadecyldimethylammonium (DHDA) monolayer yielded a substantially weaker attractive force. At 50°C (Fig. 1B), the force curve for DEDA remained identical to that measured at 25°C. Those for DHDA and DODA decreased substantially, and DHDA gave values comparable with those predicted by van der Waals theory (solid line). The force curves (Fig. 1) were integrated from double exponential functions that fit the SFA results. For example, the force curve for DODA at 25°C is

$$F/R = -0.331 e^{-D/2.1} - 0.00125 e^{-D/2.5} \quad (1)$$

where  $F$  is the force in newtons,  $R$  is the radius of curvature of the surfaces in meters,

Y.-H. Tsao and D. F. Evans, Department of Chemical Engineering and Materials Science, University of Minnesota, Minneapolis, MN 55455.  
H. Wennerström, Division of Physical Chemistry, The Chemical Center, University of Lund, S-22100 Lund, Sweden.